ACSNANO www.acsnano.org

ARTICLE

The Energy Landscape for the Self-Assembly of a Two-Dimensional DNA Origami Complex

Joshua Fern,[†] Jennifer Lu,[†] and Rebecca Schulman*[,†,‡]

[†]Chemical and Biomolecular Engineering, Johns Hopkins University, Baltimore, Maryland 21218, United States
[‡]Computer Science, Johns Hopkins University, Baltimore, Maryland 21218, United States

Supporting Information

ABSTRACT: While the self-assembly of different types of DNA origami into well-defined complexes could produce nanostructures on which thousands of locations can be independently functionalized with nanometer-scale precision, current assembly processes have low yields. Biomolecular complex formation requires relatively strong interactions and reversible assembly pathways that prevent kinetic trapping. To characterize how these issues control origami complex yields, the equilibrium constants for each possible reaction for the assembly of a heterotetrameric ring, the unit cell of a rectangular lattice, were measured using fluorescence colocalization microscopy. We found that origami interface structure controlled reaction free energies. Cooperativity, measured for the first time for a DNA nanostructure assembly reaction, was weak. Simulations of assembly kinetics suggest assembly occurs *via* parallel pathways with the primary mechanism of assembly being hierarchical: two dimers form that then bind to one another to complete the ring.

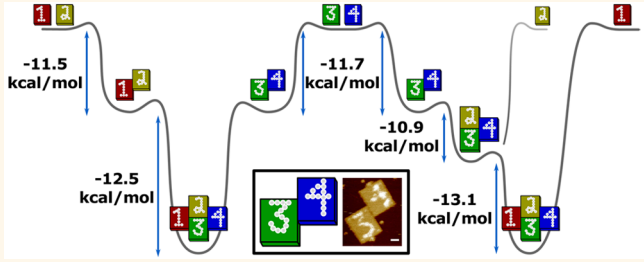

KEYWORDS: *DNA origami, DNA nanotechnology, self-assembly, equilibrium thermodynamics, reaction pathway analysis*

Methods from DNA nanotechnology offer a programmable, inexpensive way to control the structure of matter at the length scale of a few to several hundred nanometers.[1] DNA nanostructures can be applied to control the spatial configuration of enzyme cascades,[2,3] metallic nanoparticles[4] and quantum dots.[5] Furthermore, these methods can be used to construct materials with tailored optical behaviors[6−8] or as tools for cell biology research[9,10] and super-resolution microscopy.[11,12]

In many cases, the application requires the assembled structure to have a particular size and geometry such that the molecules to be positioned at each of the many potential sites on an assembled structure can be independently controlled by the binding of functionalized DNA strands with different sequences. While DNA origami enable this control,[2,3] the length scale of assembled structures with independently addressable locations across the structure is currently limited to structures only slightly larger than individual DNA origami complexes.[13−15] While somewhat larger origami can be assembled, sequence costs increase linearly with structure area.[16] Techniques such as algorithmic self-assembly make it possible to build larger structures by reusing components, lowering these costs, but impart restrictions on the patterns that are practical to assemble and errors during assembly are frequent.[17,18]

An alternative to these methods is the hierarchical assembly of origami complexes from a heterogeneous mixture of origami monomers. In such a scheme, each origami component is assembled using a largely uniform set of staple sequences and each presents a distinct set of DNA sequence-dependent interfaces that control their interactions with other components. A different origami component assembles into each location of the final structure, so that each functionalizable site in the final larger structure is uniquely addressable.

The assembly of complexes from different types of components requires control over binding rates in order to achieve high yields.[19] In contrast to the assembly of regular lattices, the assembly of defined complexes requires not only reversible interactions between assembly components, but also a set of interfaces that minimize nonspecific binding between many pairs of components that should not bind.[20] Further, the reactions involved in forming the complex must both minimize kinetic traps and stabilize the completed structure.[21−23]

A quantitative understanding of the kinetics and energetics of component-component interactions involved in an origami self-assembly process would make it possible to systematically evaluate which factors limit yields and to then improve these yields through component and reaction process design. Previous studies have examined the kinetics and thermody-

Received: August 24, 2015
Accepted: January 28, 2016
Published: January 28, 2016

DOI: 10.1021/acsnano.5b05309
ACS Nano 2016, 10, 1836−1844

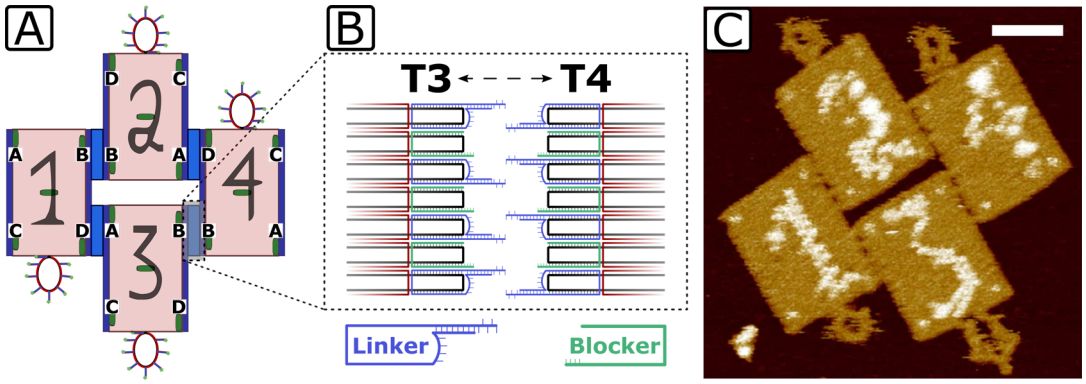

Figure 1. Multicomponent origami assembly scheme. (A) Schematic of origami showing structural staples (red), hairpins on structural staples that produce distinguishing patterns on the AFM (black letters), edge staples that control interaction between origami components (blue regions), biotin-anchoring sites (green) and fluorophore-binding sites (loop-outs). Each origami binds another origami along one interface, coded by the letters A, B, C or D. (B) Edge staples act as either "blockers" (green, 4 thymine nucleotides) or "linkers" (blue, 8 bp dsDNA + 5 bp sticky-end) for origami−origami attachment (see Supporting Figure S3). (C) AFM image of the target origami complex. In addition to the hairpins that produce visible numbers, the biotin-anchoring sites (corners and centers of each origami rectangle) and fluorophore docking sites (loops at top or bottom edge of origami) are visible. Scale bar 50 nm.

namics of the hierarchical assembly of DNA nanostructures using FRET or atomic force microscopy, but have been limited to origami 1D chain growth[14] or dimer assembly of significantly smaller nanostructures.[24−26]

Here we develop a novel assay to systematically measure the complete energy landscape of a heterogeneous self-assembly process for simple origami complexes and use it to understand Watson−Crick mediated interactions between origami components. This assay uses fluorescence microscopy and fluorophore colocalization, similar to methods previously used to detect the locations and contents of protein complexes within cells,[27] to quantify the concentrations of monomers, the many possible assembly intermediates and the target complex as an assembly process approaches equilibrium. We use this information to determine the equilibrium constants of assembly between different components and assembly intermediates, and build an energy landscape for the assembly process.

Energy landscapes are commonly used to understand how complex chemical reactions and assembly processes occur.[28] They can also be used to identify bottlenecks in supramolecular assembly[29−31] and explain how the assembly process varies under different physical conditions. Using information from these analyses, bottlenecks can be systematically overcome by changing the reaction conditions[32,33] or by designing new interactions between components or new components.[18,34,35] A better understanding of the microscopic rates of the assembly reactions could thus help optimize the assembly of origami lattice structures and, if applied to an assembly process involving different component types, could also be important for processes where rates are critical for controlling what structures are assembled.[21,23,36]

In the system we consider, the interfaces of four origami components present edges with pairs of complementary ssDNA overhangs. There are four binding interfaces that each have unique sets of sticky-end sequences; hybridization of all four interfaces produces an origami "ring" in which each origami structure is linked to two others along different interfaces. We used the assay we developed to measure the equilibrium constants for each possible combination of assembly reactants, including all combinations of origami monomer and assembly intermediates. These results suggest several important principles for reactions between origami components. In our system, origami preferentially bind along interfaces with similar structure, and the energy of interaction is not correlated with the hybridization energy of the single-stranded sticky-ends. We also find that the binding energy between two origami components does not appear to be affected by origami bound at other interfaces distant from the reaction site. Finally, we are able to directly measure the binding energy involved in ring closure, which involves reactants interacting simultaneously at multiple interface sites, and find that this set of reactions exhibit weak cooperativity. This cooperative interaction determines whether and how origami structures will demonstrate a preference for higher order structures in which most components are bound to multiple other components in the target structure. For closed complex structures, the degree of cooperativity also determines whether complete complexes are energetically favored over assembly intermediates at equilibrium.

In addition, we use the information we collect about the different assembly reactions to produce a holistic view of the assembly process. By using simulations to estimate the total amount of material produced by each reaction over time during a typical assembly process, we found that assembly of tetramer complexes most likely occurred through pathways involving the initial formation of two dimers with the lowest $\Delta G°$, followed by either the assembly of these two dimer types or the sequential addition of monomers to one of these dimers. The method we lay out using the interfaces in this paper as an example structure therefore provides a foundation for analyzing the role of component design in heterogeneous assembly processes.

RESULTS AND DISCUSSION

To determine whether the origami components with linking interfaces (Figure 1A,B, Supporting Figures S1−S5) interacted as designed, we annealed a mixture of four origami tile components from a starting temperature of 55 °C down to 25 °C at 15 min/°C. Atomic force microscopy (AFM) analysis of the mixture at 25 °C showed the presence of tetramer structures (Figure 1C), but much of the material remained as either monomers or dimers. Few trimers were observed (Supporting Figure S6).

DOI: 10.1021/acsnano.5b05309
ACS Nano 2016, 10, 1836−1844

The first step in calculating the equilibrium energy landscape of multiple pathways in an assembly process is the determination of equilibrium constants for all possible reactions in the assembly process. These equilibrium constants can be calculated using the measured relative abundances of all possible species in the reaction. While AFM has been used to characterize the yields of origami self-assembly[14,37−39] because it enables clear visualization of the structure of assemblies, quantitatively measuring binding energies between species or the relative abundances of the different species is tedious because large surface areas must be scanned serially and the resulting images generally must be analyzed manually. Because the number of intermediate complexes scales exponentially with product complex size, the amount of AFM imaging required to accurately measure the abundance of all possible complexes quickly becomes prohibitive. To characterize the assembly landscape of our reaction without an imaging bottleneck, we therefore developed a method of measuring the relative abundances of DNA origami monomers, intermediates and target complexes using fluorescence microscopy and fluorescently tagged DNA origami (Supporting Figure S7−S8). Because this method enables the identification of hundreds of origami monomers and complexes using a single epi-fluorescent image capture, it makes it possible to rapidly and accurately measure the fraction of material of many different species whose abundance may vary. To distinguish different origami species, each of the four origami were labeled with either ATTO647N (R), Cy3 (G) or ATTO488 (B) fluorophores or kept unlabeled in a given reaction. The composition of the complex could then be determined by the combination of fluorophores it possesses.

One potential source of error in our fluorescence measurements is that when the density of origami on the glass surface is high, components can land near one another by chance so that they appear bound to one another. We used simulations to determine how often these events would occur and the amount it would skew our measurements of complex abundances using fluorescence colocalization (Supporting Figures S9−S10). We found that for typical densities of origami components on slides, about 3% of origami components that were unbound appeared to be in assemblies.

To verify that our fluorescence colocalization microscopy technique could be used to characterize the relative abundances of origami and origami complexes, we compared the results of the technique with measurements of the abundances of complexes taken using atomic force microscopy. We mixed sets of two origami that were designed to bind to one another, heated them to 55 °C and then slowly cooled them using an annealing schedule that ensured the reaction had approached equilibrium between 50° and 25 °C (Supporting Notes S1−S2). Each of the two origami monomers were labeled with a different fluorophore so that static fluorescence micrographs of surface-bound origami provided a 2D representation of reaction composition (Figure 2A). The relative fraction of species in each possible configuration (the two monomers or the dimer) was determined by counting the number of objects that appeared in one or two fluorophore channels (Figure 2B). We compared the reaction compositions of a two-component reaction mixture measured using our microscopy methods with those from the same reaction characterized using AFM scans and found that the measured fraction of material in a dimer complex measured using our fluorescence assay and AFM micrographs were similar to one another, suggesting that the

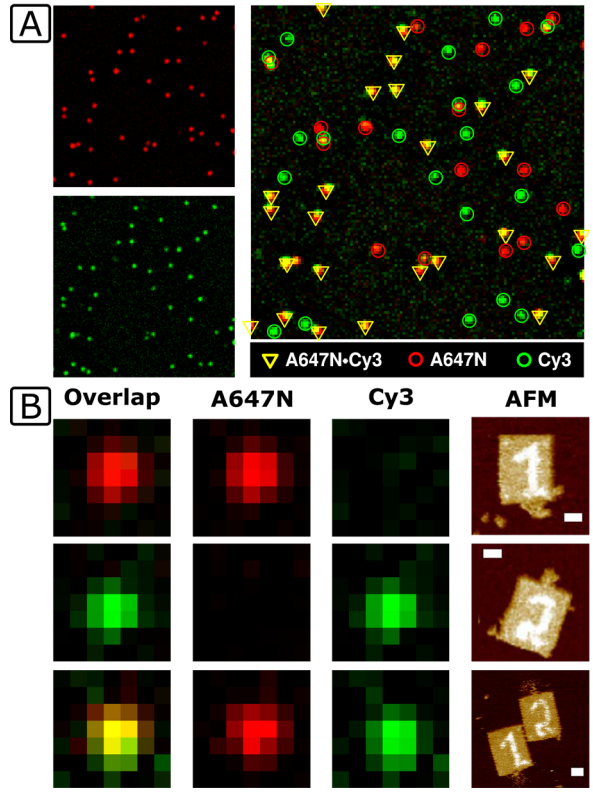

Figure 2. Multicolor fluorophore labeling of different origami components allows the assembly state of origami complexes to be determined from multicolor fluorescence micrographs. (A) The two origami tile types are labeled with two different fluorophore types for the assembly of T1-ATTO647N and T2-Cy3 into a T12 dimer. Pixel locations of apparent origami structures are visualized in individual fluorescence channels (red and green). Fluorescent objects that appear in multiple channels are origami assemblies (right image, labeled by colored shapes designating which channels). Supporting Note S3 details the algorithm used to detect and count fluorescent objects. Image sizes: 21.4 × 21.4 μm. (B) Example fluorescent origami assembly species, both in individual channels and overlays, for objects in one or two channels and an AFM representation of the specified fluorescent object. Size of each fluorescent image: 1.2 × 1.2 μm; AFM scale bars: 25 nm.

fluorescence microscopy assay we developed can be used to quantitatively measure the fraction of material in different reaction states (Supporting Figures S11−S13, Supporting Table S1).

After verifying that our assay could be used to measure the fraction of material in different configurations close to equilibrium, we used it to find equilibrium yields in all possible reactions involving two or three binding species. Since there was a 1:1 ratio between the possible number of fluorophore types (3) and the number of origami components (up to 3 in dimerization and trimerization reaction mixtures), the fraction of material values for all species in a reaction were directly calculated from counts of objects in the fluorescent images (Supporting Figure S14, Figure 3A).

Previous experiments have shown qualitatively that the amount of binding between origami can be dependent on the structure of the origami components,[37] which can vary across a rectangular origami structure because of asymmetries in either crossover patterns or sequence.[40] The four interfaces of the origami components we designed, therefore, might be expected to bind to one another in reactions with different equilibrium

DOI: 10.1021/acsnano.5b05309
ACS Nano 2016, 10, 1836−1844

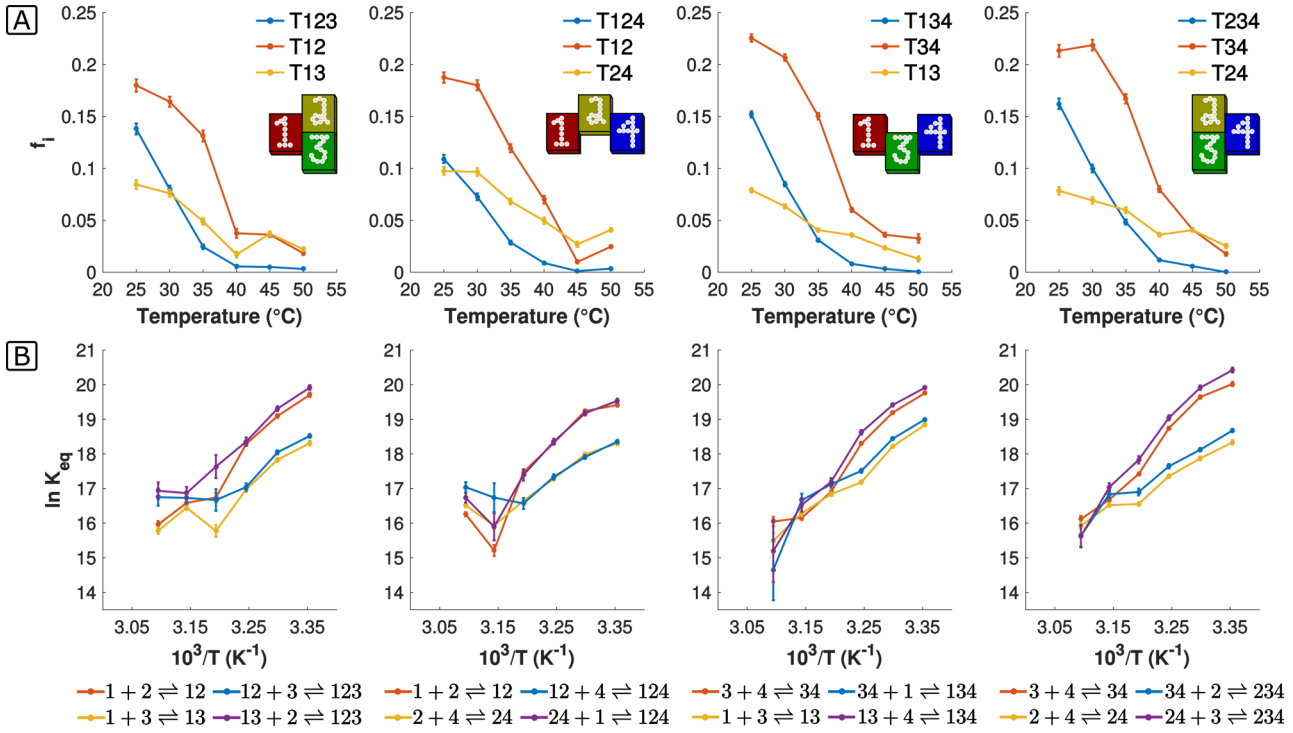

Figure 3. Distribution of assembly material among potential species in reactions involving 3 origami components close to thermodynamic equilibrium at a range of temperatures and the corresponding equilibrium constants for the assembly reactions. (A) The fraction of assembly material (f_i) in four reaction mixtures involving three of the four origami components (left to right): 1−2−3, 1−2−4, 1−3−4 and 2−3−4. (B) Van't Hoff plots (log of the equilibrium constant *vs* inverse temperature) for the possible reactions between the components for the reactions in (A). Equilibrium constants for reactions where binding occurs between the same types of interfaces (1−2 and 3−4) are larger than those for reactions where binding occurs between different interface types (1−3 and 2−4). Nonlinear behavior in the Van't Hoff plots precluded the calculation of standard enthalpy and entropy changes for each assembly reaction. Here and elsewhere, error bars were calculated as described in Supporting Note S5.

constants, even if the sticky-end sequences that hybridized during binding were the same. In support of these ideas, we found that the K_{eq} of a reaction was dependent upon which interfaces of the origami were interacting (Figure 3B). Relatively strong binding was observed between origami monomer pairs T1-T2 and T3-T4, where binding occurs between two origami interfaces with identical structure - interface "B" (Figure 1A). Weaker interactions were observed between T1-T3 and T2-T4, where binding occurs between the dissimilar origami interfaces "D" and "A". In contrast, the hybridization energy for each interface's binding predicted by considering the hybridization of the sticky-end sequences using the nearest-neighbor model[41] did not correlate with the measured equilibrium binding constants for origami binding, as free energies of binding predicted using this method were very close to equal (Supporting Table S2).

In protein assembly, allosteric interactions between components are common. Allostery implies that when two components bind, the conformations of the components change, altering the binding energy between these components and future binding partners. To determine whether allosteric interactions were present in the assembly of origami complexes, presumably because of conformational changes incurred by the origami as they hybridize, we compared equilibrium constants of a dimerization reaction in the presence or absence of a third origami component capable of binding a secondary interface. For example, in the T1+T2, T2+T4 and T1+T2+T4 reaction systems, we found that the addition of a third component to a reaction mixture did not have a significant effect on the K_{eq} of a reaction, implying that allosteric interactions do not have a major role in origami−origami binding here (Supporting Figures S16−S17).

The number of unique fluorophore types available to a conventional microscopy system is often limited to three or four due to the spectral overlaps between fluorophores and limitations in available light filter sets. This limitation is an obstacle to the use of the described assay for the analysis of reaction mixtures with more components than fluorophore types. To scale our technique for measuring the equilibrium constants of individual reactions to systems with more than three components, we developed a method to measure the contents of reaction mixtures by running the same reaction several times using different labeling schemes for the components in each reaction, and combining the data from these reactions to find the fraction of material in each possible monomer or complex. Because the fluorophore labels on the components did not affect their binding behavior (Supporting Figure S11), we assumed that the equilibrium constants in each of the reaction mixtures were the same. To study how the fraction of assembly material was distributed among the possible species in a reaction to form a heterotetrameric ring (Figure 1), we performed three assembly reactions and measured the distribution of colocalized fluorophores in each reaction mixture. In two out of the three reaction mixtures, three of the origami were labeled with three different types of fluorophores and a fourth origami was not labeled (unlabeled origami were denoted with an "N"). In the third reaction

DOI: 10.1021/acsnano.5b05309
ACS Nano 2016, 10, 1836−1844

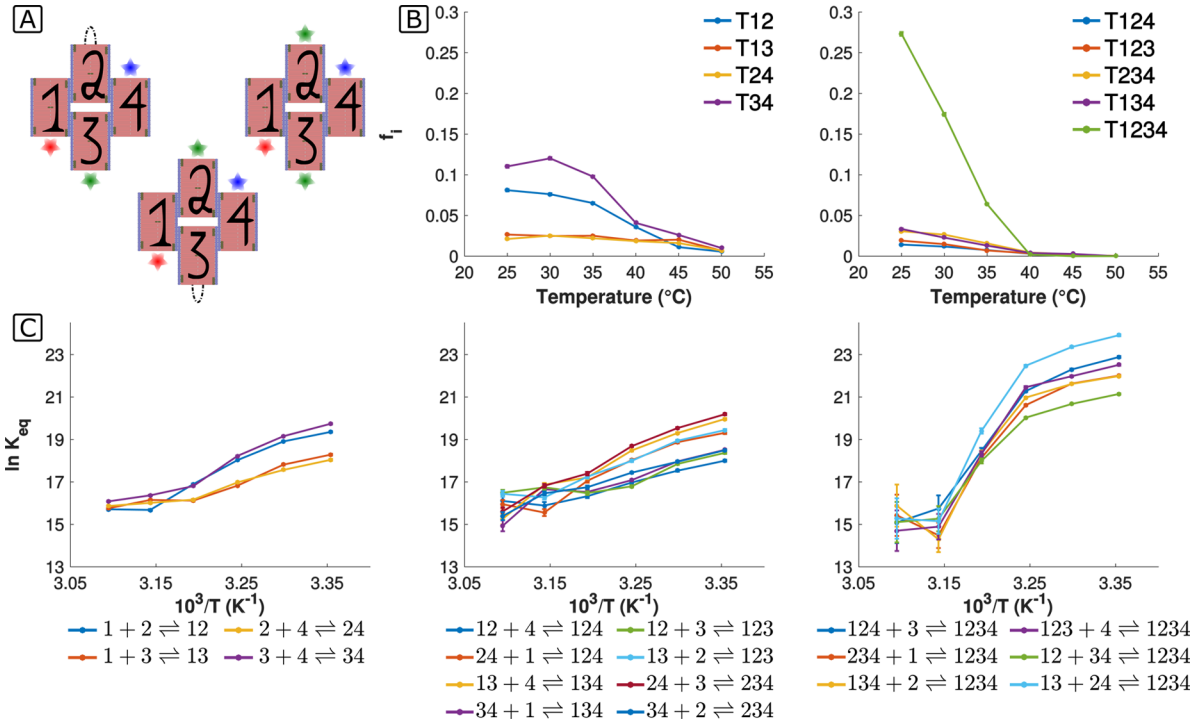

Figure 4. Determination of the equilibrium constants for a four-component origami assembly reaction. (A) Example set of origami component labeling schemes used when measuring the distribution of complexes in four-component assembly: either T2, T3 or both T2 and T3 were labeled with a Cy3 fluorophore in three separate experiments (these labeling schemes were termed T1234-RNGB/RGNB/RGGB respectively). We also characterized the four component assembly process using the labeling schemes T1234-NRBG/GRBN/GRBG. Comparison of the results predicted using these two labeled schemes were also used identify and correct numerical instabilities in our analysis process (Supporting Notes S7–S8). (B) Combining the fluorescent object abundances from each reaction mixture enabled the calculation of the fraction of reaction material (f_i) of all 15 possible species (see text). At 25 °C, the majority of components existed as monomers (~33%) or tetramers (~30%). (C) Equilibrium constants for the 18 assembly reactions. Tetramerization reactions showed higher equilibrium constants than dimerization and trimerization reactions at every measured temperature, suggesting the presence of cooperative interactions. Data in (B) and (C) were determined using both the RNGB/RGNB/RGGB and NRBG/GRBN/GRBG labeling schemes (see Supporting Note S5).

mixture, the fourth origami was labeled with the same type of fluorophore as one of the other origami (Figure 4A).

We counted the abundance of each of the colocalized fluorescent objects in each experiment in the same manner as in the two- and three-component mixtures (*e.g.*, the number of objects in each fluorescent channel at the same location in each of the labeling schemes). The abundances of each possible combination of colocalized fluorescent labels in each of the three experiments were then related by mass balance equations describing the possible fluorescent objects representing a given assembly species (Supporting Table S3). For example, in the T1234-RNGB scheme, an object that fluoresces in the red and green channels represents either a T13 or a T123 species due to the "2" origami being unlabeled, so the fraction of material that fluoresces in red and green is the sum of the fractions of the material that are either T13 or T123. Assuming that the fraction of material of each species does not change between reaction mixtures, the mixtures with different labels will each constrain our knowledge about the values of these abundances, making it possible to calculate them given all of the information from the three reactions with different fluorophore labeling schemes. We used a least-squares solver using the mass balance equations to find the best fit to the fraction of material of the possible species, with the bounding constraints that the fraction of material of each species must be nonnegative (Supporting Note S7). However, we found that this method for determining the fraction of material and equilibrium constants was difficult numerically: the fits to the fraction of material for each species were highly dependent on the assumption that the concentration of each origami component was exactly the same in each experiment because, in practice, the concentration of the origami components varied slightly between the reaction mixtures because of effects such as pipetting error (Supporting Figure S18).

To estimate the concentrations of the different species in a manner that was less sensitive to slight measurement variations between experiments, we modified the system of equations used in our analysis. On the basis of our observations that reactions between origami components do not exhibit allostery, we assumed that the equilibrium constants for the dimerization and trimerization reactions in the four-component mixture were close to those for the reactions measured in the two- and three-component mixtures. We used this assumption to constrain the equilibrium constants for the dimerization and trimerization reactions to be close to those we had previously measured. The resulting fits produced the same results for different subsets of experiments, indicating that they were not as sensitive to small variations between different assembly reactions (Supporting Note S8, Supporting Figure S19). The resulting measured fractions of material and equilibrium constants are shown in Figure 4B,C.

Measuring the equilibrium constants for the reactions that form four-component origami complexes allowed us to determine the binding energy for reactions that formed the

DOI: 10.1021/acsnano.5b05309
ACS Nano 2016, 10, 1836–1844

target complex (Figure 4C). These reactions, which included those between a monomer and trimer and those between two origami dimers, allowed two origami interfaces to interact simultaneously. At every temperature, the K_{eq} for each of these reactions was larger than the K_{eq} measured for any dimerization and trimerization reaction, suggesting the presence of cooperative interactions. That is, the reaction of the components by multiple origami binding interfaces increased the energy of interaction (lower $\Delta G°$). Because of the symmetry in the design of the origami complex assembly, all of the trimer-monomer reactions involved both B−B and A−D interface binding (*e.g.*, T123+T4 reaction has T3-T4 and T2-T4 interface binding reactions) and resulted in equally balanced K_{eq} values. However, the reactions between two dimers consisted of either two B−B interface reactions (T13+T24) or two A−D interface reactions (T12+T34). With these reactions, there was a marked difference in equilibrium constants; the B−B interface reaction had about a 20-fold higher K_{eq} than the A−D interface reactions. This followed the pattern observed earlier in dimerization and trimerization reactions where B−B interface reactions had a greater equilibrium constant in the studied system as compared with A−D interface binding reactions.

We used the equilibrium constants for all possible reactions in the four-origami component system and kinetic assembly simulations to produce an energy landscape for assembly. This landscape shows which relative pathways from origami monomers to the target complex were the most energetically favorable (Figure 5). The energy landscape is important because its shape can determine the yield of assembly;[28,29] in particular, one potential principle for design is the idea that a biased assembly pathway, in which a single assembly process tends to be followed, is an efficient method for self-assembling complexes.[21,42]

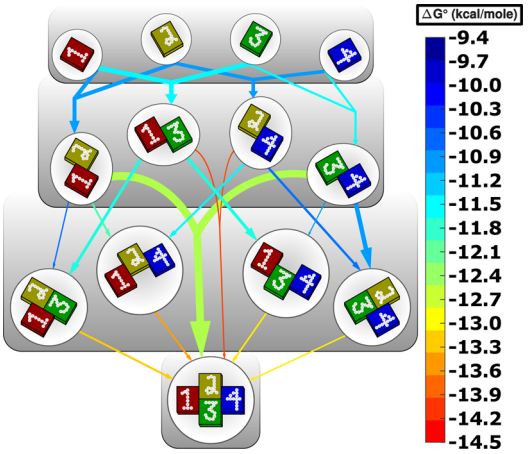

Figure 5. Assembly landscape for a four-component origami assembly reaction. Pathways in the self-assembly of a four-component nanostructure are shown for assembly at 25 °C. Each arrow represents a possible reaction between components with the product complex at the arrow's end. The line color is the calculated free energy change from experimental measurements using $\Delta G° = -RT \ln K_{eq}$ (from blue to red is more negative) and the width of the line indicates the relative amount of material generated by each reaction in kinetic simulations. For clarity, arrows for monomers are omitted for reactions involving a monomer and a larger assembly.

We created a simple kinetic simulation of the assembly process to understand how assembly of tetramer complexes might occur. Following models and experiments analyzing DNA tile crystallization[17] and DNA origami oligomerization,[39] we considered how assembly would occur if the system had a single on-rate for all reactions. Using this on-rate, we then calculated the off-rate for each reaction using the equilibrium constants that we experimentally measured, and used these rates in a mass-action kinetic simulation of the assembly process of the four origami components (Supporting Note S9, Supporting Figures S20−S22).

We calculated the relative amount of material produced by each reaction in our simulations. For dimerization reactions, the major products generated were T12 and T34, and because the concentrations of these two dimer species were much higher than the other two dimers, the reaction rates for subsequent reactions from T12 or T34, either when adding a third monomer or the T12+T34 dimer−dimer reaction, were also large, despite those interfaces having lower binding energies. The most prevalent tetramerization reaction in our simulations was T12+T34, forming about 2× more tetramers at 25 °C than the next most favored reaction, T234+T1 (Supporting Figure S22). While T12+T34 was the dominant tetramerization reaction at temperatures less than 40 °C, the dominant assembly pathway varied with temperature (Supporting Figure S22). An energy diagram, depicting the free energy and the relative amount of produced complex for each reaction at 25 °C is shown in Figure 5.

CONCLUSION

In this paper, we develop a method using standard fluorescence microscopy techniques to determine the equilibrium constants for the assembly of heterogeneous DNA origami complexes. The techniques outlined are straightforward for the complete analysis of small assembly reactions in which each component can be labeled with a different fluorophore type, and can also be extended to include more components by repeating reactions with different labeling combinations, and by using mass balance equations and the equilibrium constants measured in simpler reactions. These techniques could also be used to characterize the thermodynamics of 3-dimensional origami assembly processes.

The energy landscape we determined demonstrates important principles that govern the energetics of origami complex assembly, and can be used to increase the yield and efficiency of self-assembly. We found that the energy of interaction between different components appeared to be controlled not by the specific sequences in the Watson−Crick binding pairs, but by the structure of the origami interface. This result suggests that, despite the importance of sequence effects in DNA hybridization, in the assembly of larger origami structures the structure of the interfaces largely determines binding energies, even when the binding process is actually mediated by DNA hybridization. These results expand upon studies of smaller DNA nanostructures where the architecture of small DNA tiles impacts the thermodynamics and kinetics of dimerization.[26,43] It would therefore be interesting to characterize how the structure (*e.g.*, rigidity) of origami and their interfaces affect the on-rate of origami−origami binding.

Understanding how to assemble DNA origami structures using Watson−Crick base-pairing is important because, while blunt-end base stacking is an alternative method to hierarchically self-assemble origami into larger structures, there are a

DOI: 10.1021/acsnano.5b05309
ACS Nano 2016, 10, 1836−1844

relatively small number of distinct blunt-end stacking interfaces[14] and the resulting structures would be difficult to stabilize *via* processes such as enzymatic ligation.

Additionally, explicit consideration of the structure of origami components at the nanometer scale as predicted in simulation[44,45] or experiment[46] could be used to build higher-yield tunable interfaces between origami components.[47] The fact that binding energies are so dependent on structure may also make it possible to use these sorts of measurements to quickly and inexpensively test hypotheses about the average structure and the ensemble of structures of particular origami assemblies.[44]

Our techniques further suggest a way to explicitly measure cooperative interactions between multiple component types. In the case of homogeneous assembly, these methods would make it possible to measure cooperativity easily to aid in the construction of large lattices. Some degree of cooperativity is required for the assembly of regular crystals with few defects[17,48] and also, in the case of closed complex structures like those studied here, controls the stability of the final complex. Cooperativity is also important for the control of the self-assembled product in processes such as algorithmic self-assembly.[17]

Finally, the technique developed here allows the elucidation of the complete energy landscape for assembly and therefore can be important for a systems-level analysis of origami component assembly processes. While the development of principles for the self-assembly of complexes is still being elucidated,[21−23,36] it is clear that the ensemble of binding energies and how they are distributed between reactions is a major determinant of assembly speed and yield. The ability to measure all of the binding energies for a single assembly process, and perhaps to also tune these energies by designing alternative pairs of interfaces, will be important for a rational, reliable route to the self-assembly of origami complexes and more generally, to the hierarchical self-assembly of DNA structures that bridge different length scales.

MATERIALS AND METHODS

Origami Design. The components of the self-assembly process were four two-dimensional rectangle origami, each composed of 191 staple strands with sequence complementarity to bacteria-phage M13mp18 DNA (Figure 1, Supporting Figure S1−S3). Each origami was 32 helices wide and 219 bases long giving a size of about 101 × 75 nm as measured by atomic force microscopy. The helical twist of the origami structure was set at 10.43 bp/turn using selective deletion every 48 bases and by offsetting staple termination points along the length of the origami.[14] DNA hairpins inserted in the staple sequences in patterns of a "1", "2", "3," or "4" on the origami were used as distinguishing markers and visualized using atomic force microscopy. Origami used in fluorescence microscopy experiments also contained hairpins. Five staple strands, spaced across the origami, contained an additional docking region sequence on which a biotinylated DNA strand hybridized. These biotinylated strands enabled origami assemblies to attach to a Neutravidin coated glass surface. Eight other strands hybridized to the part of the M13 not complementary to staple strands and provided docking sites for fluorophore-labeled strands (Supporting Figure S7). Staples along the edges of the origami were classified as either "blockers" or "linkers." A blocker edge staple had a 4 nucleotide poly-T sequence extending from the origami edge designed to minimize nonspecific interactions between origami and inhibit excess linker staples in solution from binding to the origami and acting as additional sites for mediating origami−origami interaction (Figure 1B, Supporting Figure S3). Linker staples produced an overhang on the origami components consisting of an eight-base region in which the two regions of the same strand hybridized with one another followed by five nucleotides complementary to the same region on one other linker. A specific interface for origami−origami binding was comprised of four linker and three blocker staples. On each origami, linkers extended from two of the four possible interfaces (Figure 1A,B) and were designated as interface "A" (top-left side), "B" (top-right side) or interface "D" (bottom-right side). Interface "C" was not involved in linking on any of the components and only contained blocker edge staples.

Origami Preparation. DNA solutions for each origami were prepared as mixtures of scaffold strands (M13mp18, Bayou Biolabs), staple strands and labeling strands (Integrated DNA Technologies, Inc.). Staple strands consisted of structural, edge (linkers and blockers), fluorophore docking, and anchor docking strands. DNA strands containing either a fluorophore (ATTO647N, Cy3, or ATTO488) or a biotin molecule hybridized to docking sites on the origami. Origami that were not fluorescently labeled were prepared with a DNA strand that lacked a fluorophore but had the same sequence as the fluorophore labeling strands. These additional strands prevented excess, free fluorescently labeled strands from attaching to unlabeled origami. Hereafter, origami are noted by their number after a T (for origami tile) and the color of their fluorescent label, *e.g.*, T1-R for an ATTO647N labeled Tile-1 origami. Unlabeled origami have an "N" label, *e.g.*, T1-N. Origami stock solutions were prepared as 20 nM scaffold strand, 200 nM structural and anchor docking staples, 60 nM linkers, 200 nM blockers, 1200 nM biotinylated strands, 60 nM fluorophore docking strands, and 600 nM fluorophore-labeled strands. Before assembly, each monomer origami was prepared by annealing all above listed strands in TAE/Mg^{2+} buffer (40 mM Tris-acetate, 1 mM EDTA, supplemented with 12.5 mM magnesium acetate) from 90 to 20 °C at 1 °C/min using an Eppendorf Nexus thermocycler. Origami stock solutions were used without purification. AFM scans showed that <4% of all origami monomers were malformed (*e.g.*, broken or hairpins were indiscernible).

Assembly of Origami into Complexes and Reaction Equilibration. To assemble origami complexes, origami monomers were mixed in equal volumes from stock solutions to produce a mixture containing 5 nM of each origami type. This mixture was separated into aliquots, one per sampling temperature, and loaded into a thermocycler. During self-assembly, these mixtures were first heated to 55 °C for 20 min to melt any origami complexes (and not origami components themselves, see Supporting Note S1) that might have formed during the initial mixing of the origami monomers at room temperature. After 20 min, the mixtures were cooled from 55 to 25 °C at 15 min/°C, a rate at which origami−origami binding reactions were expected to equilibrate at each temperature step (Supporting Note S2).

Origami Assembly Reaction Sampling. In increments of 5 °C between 50 and 20 °C, the composition of the reaction was measured using fluorescence microscopy. Fifteen minutes prior to sampling, tubes containing 200 μL of TAE/Mg^{2+} were added to a dry heater at the sampling temperature; the contents of these tubes were used to dilute the reaction samples. After quickly transferring individual reaction tubes to the dry heater, the solutions in the tubes were diluted by mixing 1 μL of the reaction solution with the dilution tube in the dry heater. For glass bottom dishes, 20 μL of diluted solution was added quickly after mixing to the Neutravidin treated surface containing 100 μL of TAE/Mg^{2+} and incubated for 3 s. Fifty microliters of diluted solution was incubated for 8 s on coverslips. After incubation, surfaces were quickly washed with TAE/Mg^{2+} to remove unbound origami and stored in TAE/Mg^{2+} until imaging. The attachment of origami using biotin-Neutravidin linkages ensured that origami could not travel on the surface or return to solution, so the structure of the monomers and complexes were expected to remain stable between sample preparation and imaging a few minutes to hours later. Fluorescent imaging was conducted on an Olympus IX71 inverted microscope with 1.6× magnification using a 60×/1.45 NA oil immersion objective (96x total magnification) and a cooled Andor iXon3 CCD camera using custom image-capture software. Three filter sets (Supporting Table S6) were used to separately image origami

DOI: 10.1021/acsnano.5b05309
ACS Nano 2016, 10, 1836−1844

labeled with ATTO647N (red, R), ATTO488 (blue, B) or Cy3 (green, G).

Preparation of Surfaces for Fluorescence Microscopy. Glass coverslips (VWR) or glass bottom dishes (*In Vitro* Scientific) were cleaned *via* sonication with 10 w/v% NaOH for 25 min. After washing with Milli-Q pure water, surfaces were treated with 50 μL of 0.5 mg/mL Biotin-BSA (Sigma-Aldrich) in TNT buffer (10 mM Tris-HCL, 0.1 M NaCl, 0.05% Tween-20 at pH 7.5) for 30 min. After washing three times with TNT, glass surfaces were treated with 50 μL of 0.5 mg/mL Neutravidin (Thermo Scientific) in TNT buffer for 15 min. Excess Neutravidin was removed by washing the surfaces four times with TAE/Mg^{2+} buffer. All surfaces were prepared and used for microscopy measurements on the same day.

Atomic Force Microscopy. For AFM imaging, sample tubes were removed from the thermocycler and transferred to a heated glovebox using a dry heater (all set to the reaction temperature being characterized). Inside the glovebox, 10 μL of TAE/Mg^{2+} was added to a small, freshly cleaved mica puck. Four microliters of reaction sample solution was added to the puck and incubated for 1 min followed by washing with TAE/Mg^{2+} four times to remove excess DNA strands and origami species. Finally, 60 μL of TAE/Mg^{2+} was added and the puck was transferred to the AFM. All imaging was conducted using a Bruker Dimension Icon in ScanAsyst mode with a sharp nitride lever tip (SNL-10, tip C, Bruker) cantilever under fluid conditions.

ASSOCIATED CONTENT

Supporting Information

The Supporting Information is available free of charge on the ACS Publications website at DOI: 10.1021/acsnano.5b05309.

DNA sequences, additional methods, notes and experiments referenced in the paper. (PDF)

AUTHOR INFORMATION

Corresponding Author

*E-mail: rschulm3@jhu.edu.

Notes

The authors declare no competing financial interest.

ACKNOWLEDGMENTS

The authors would like to thank J. Zenk for component sequence design and assistance with AFM measurements, A. M. Mohammed for assistance in the fluorophore labeling and A. Cangialosi for helpful discussions and advice on the manuscript. This work was supported by NSF grants CCF-1161941 and CMMI-1253876. We also acknowledge DOE BMES grant DE-SC0010595 for some materials and supplies.

REFERENCES

(1) Rothemund, P. W. K. Folding DNA to Create Nanoscale Shapes and Patterns. *Nature* **2006**, *440*, 297−302.
(2) Wilner, O. I.; Weizmann, Y.; Gill, R.; Lioubashevski, O.; Freeman, R.; Willner, I. Enzyme Cascades Activated on Topologically Programmed DNA Scaffolds. *Nat. Nanotechnol.* **2009**, *4*, 249−254.
(3) Fu, J.; Yang, Y. R.; Johnson-Buck, A.; Liu, M.; Liu, Y.; Walter, N. G.; Woodbury, N. W.; Yan, H. Multi-Enzyme Complexes on DNA Scaffolds Capable of Substrate Channeling with an Artificial Swinging Arm. *Nat. Nanotechnol.* **2014**, *9*, 531.
(4) Chao, J.; Lin, Y.; Liu, H.; Wang, L.; Fan, C. DNA-Based Plasmonic Nanostructures. *Mater. Today* **2015**, *18*, 326.
(5) Samanta, A.; Deng, Z.; Liu, Y. Infrared Emitting Quantum Dots: DNA Conjugation and DNA Origami Directed Self-Assembly. *Nanoscale* **2014**, *6*, 4486−4490.
(6) Kuzyk, A.; Schreiber, R.; Fan, Z.; Pardatscher, G.; Roller, E.-M.; Högele, A.; Simmel, F. C.; Govorov, A. O.; Liedl, T. DNA-Based Self-Assembly of Chiral Plasmonic Nanostructures with Tailored Optical Response. *Nature* **2012**, *483*, 311−314.
(7) Ding, B.; Deng, Z.; Yan, H.; Cabrini, S.; Zuckermann, R. N.; Bokor, J. Gold Nanoparticle Self-Similar Chain Structure Organized by DNA Origami. *J. Am. Chem. Soc.* **2010**, *132*, 3248−3249.
(8) Tan, S. J.; Campolongo, M. J.; Luo, D.; Cheng, W. Building Plasmonic Nanostructures with DNA. *Nat. Nanotechnol.* **2011**, *6*, 268−276.
(9) Schüller, V. J.; Heidegger, S.; Sandholzer, N.; Nickels, P. C.; Suhartha, N. a.; Endres, S.; Bourquin, C.; Liedl, T. Cellular Immunostimulation by CpG-Sequence-Coated DNA Origami Structures. *ACS Nano* **2011**, *5*, 9696−9702.
(10) Shaw, A.; Lundin, V.; Petrova, E.; Fördős, F.; Benson, E.; Al-Amin, A.; Herland, A.; Blokzijl, A.; Högberg, B.; Teixeira, A. I. Spatial Control of Membrane Receptor Function Using Ligand Nanocalipers. *Nat. Methods* **2014**, *11*, 841−846.
(11) Schmied, J. J.; Raab, M.; Forthmann, C.; Pibiri, E.; Wünsch, B.; Dammeyer, T.; Tinnefeld, P. DNA Origami-Based Standards for Quantitative Fluorescence Microscopy. *Nat. Protoc.* **2014**, *9*, 1367−1391.
(12) Steinhauer, C.; Jungmann, R.; Sobey, T. L.; Simmel, F. C.; Tinnefeld, P. DNA Origami as a Nanoscopic Ruler for Super-Resolution Microscopy. *Angew. Chem., Int. Ed.* **2009**, *48*, 8870−8873.
(13) Rajendran, A.; Endo, M.; Katsuda, Y. Programmed Two-Dimensional Self-Assembly of Multiple DNA Origami Jigsaw Pieces. *ACS Nano* **2011**, *5*, 665−671.
(14) Woo, S.; Rothemund, P. W. K. Programmable Molecular Recognition Based on the Geometry of DNA Nanostructures. *Nat. Chem.* **2011**, *3*, 620−627.
(15) Zhao, Z.; Liu, Y.; Yan, H. Organizing DNA Origami Tiles into Larger Structures Using Preformed Scaffold Frames. *Nano Lett.* **2011**, *11*, 2997−3002.
(16) Marchi, A. N.; Saaem, I.; Vogen, B. N.; Brown, S.; LaBean, T. H. Towards Larger DNA Origami. *Nano Lett.* **2014**, *14*, 5740−5747.
(17) Rothemund, P. W. K.; Papadakis, N.; Winfree, E. Algorithmic Self-Assembly of DNA Sierpinski Triangles. *PLoS Biol.* **2004**, *2*, e424.
(18) Barish, R. D.; Schulman, R.; Rothemund, P. W. K.; Winfree, E. An Information-Bearing Seed for Nucleating Algorithmic Self-Assembly. *Proc. Natl. Acad. Sci. U. S. A.* **2009**, *106*, 6054−6059.
(19) Deeds, E. J.; Bachman, J. A.; Fontana, W. Optimizing Ring Assembly Reveals the Strength of Weak Interactions. *Proc. Natl. Acad. Sci. U. S. A.* **2012**, *109*, 2348−2353.
(20) Kim, K. N.; Sarveswaran, K.; Mark, L.; Lieberman, M. Comparison of Methods for Orienting and Aligning DNA Origami. *Soft Matter* **2011**, *7*, 4636.
(21) Zenk, J.; Schulman, R. An Assembly Funnel Makes Biomolecular Complex Assembly Efficient. *PLoS One* **2014**, *9*, e111233.
(22) Hedges, L.; Mannige, R.; Whitelam, S. Growth of Equilibrium Structures Built from a Large Number of Distinct Component Types. *Soft Matter* **2014**, *10*, 6404−6416.
(23) Jacobs, W. M.; Reinhardt, A.; Frenkel, D. Rational Design of Self-Assembly Pathways for Complex Multicomponent Structures. *Proc. Natl. Acad. Sci. U. S. A.* **2015**, *112*, 6313.
(24) Nangreave, J.; Yan, H.; Liu, Y. Studies of Thermal Stability of Multivalent DNA Hybridization in a Nanostructured System. *Biophys. J.* **2009**, *97*, 563−571.
(25) Saccà, B.; Meyer, R.; Feldkamp, U.; Schroeder, H.; Niemeyer, C. M. High-Throughput, Real-Time Monitoring of the Self-Assembly of DNA Nanostructures by FRET Spectroscopy. *Angew. Chem., Int. Ed.* **2008**, *47*, 2135−2137.
(26) Jiang, S.; Yan, H.; Liu, Y. Kinetics of DNA Tile Dimerization. *ACS Nano* **2014**, *8*, 5826−5832.
(27) Dunn, K. W.; Kamocka, M. M.; McDonald, J. H. A Practical Guide to Evaluating Colocalization in Biological Microscopy. *Am. J. Physiol. Cell Physiol.* **2011**, *300*, C723−C742.
(28) Wales, D. J.; Bogdan, T. V. Potential Energy and Free Energy Landscapes. *J. Phys. Chem. B* **2006**, *110*, 20765−20776.

DOI: 10.1021/acsnano.5b05309
ACS Nano 2016, 10, 1836−1844

(29) Bryngelson, J. D.; Onuchic, J. N.; Socci, N. D.; Wolynes, P. G. Funnels, Pathways, and the Energy Landscape of Protein Folding: A Synthesis. *Proteins: Struct., Funct., Genet.* **1995**, *21*, 167−195.
(30) Pandey, S.; Ewing, M.; Kunas, A. Algorithmic Design of Self-Folding Polyhedra. *Proc. Natl. Acad. Sci. U. S. A.* **2011**, *108*, 19885.
(31) Gröschel, A. H.; Schacher, F. H.; Schmalz, H. Precise Hierarchical Self-Assembly of Multicompartment Micelles. *Nat. Commun.* **2012**, *3*, 710.
(32) Delic, M.; Göngrich, R.; Mattanovich, D.; Gasser, B. Engineering of Protein Folding and Secretion-Strategies to Overcome Bottlenecks for Efficient Production of Recombinant Proteins. *Antioxid. Redox Signaling* **2014**, *21*, 414−437.
(33) Zimmermann, V.; Beller, M.; Kragl, U. Modelling the Reaction Course of a Dynamic Kinetic Resolution of Amino Acid Derivatives: Identifying and Overcoming Bottlenecks. *Org. Process Res. Dev.* **2006**, *10*, 622−627.
(34) Mohammed, A. M.; Schulman, R. Directing Self-Assembly of DNA Nanotubes Using Programmable Seeds. *Nano Lett.* **2013**, *13*, 4006−4013.
(35) Lai, Y.-T.; King, N. P.; Yeates, T. O. Principles for Designing Ordered Protein Assemblies. *Trends Cell Biol.* **2012**, *22*, 653−661.
(36) Murugan, A.; Zou, J.; Brenner, M. P. Undesired Usage and the Robust Self-Assembly of Heterogeneous Structures. *Nat. Commun.* **2015**, *6*, 6203.
(37) Li, Z.; Wang, L.; Yan, H.; Liu, Y. Effect of DNA Hairpin Loops on the Twist of Planar DNA Origami Tiles. *Langmuir* **2012**, *28*, 1959−1965.
(38) Liu, W.; Zhong, H.; Wang, R.; Seeman, N. C. Crystalline Two-Dimensional DNA-Origami Arrays. *Angew. Chem.* **2011**, *123*, 278−281.
(39) Chen, H.; Weng, T. W.; Riccitelli, M. M.; Cui, Y.; Irudayaraj, J.; Choi, J. H. Understanding the Mechanical Properties of DNA Origami Tiles and Controlling the Kinetics of Their Folding and Unfolding Reconfiguration. *J. Am. Chem. Soc.* **2014**, *136*, 6995−7005.
(40) Li, Z.; Liu, M.; Wang, L.; Nangreave, J.; Yan, H.; Liu, Y. Molecular Behavior of DNA Origami in Higher-Order Self-Assembly. *J. Am. Chem. Soc.* **2010**, *132*, 13545−52.
(41) SantaLucia, J. A Unified View of Polymer, Dumbbell, and Oligonucleotide DNA Nearest-Neighbor Thermodynamics. *Proc. Natl. Acad. Sci. U. S. A.* **1998**, *95*, 1460−1465.
(42) Marsh, J. a.; Hernández, H.; Hall, Z.; Ahnert, S. E.; Perica, T.; Robinson, C. V.; Teichmann, S. a. Protein Complexes Are under Evolutionary Selection to Assemble *via* Ordered Pathways. *Cell* **2013**, *153*, 461−470.
(43) Nangreave, J.; Yan, H.; Liu, Y. DNA Nanostructures as Models for Evaluating the Role of Enthalpy and Entropy in Polyvalent Binding. *J. Am. Chem. Soc.* **2011**, *133*, 4490.
(44) Kim, D. N.; Kilchherr, F.; Dietz, H.; Bathe, M. Quantitative Prediction of 3D Solution Shape and Flexibility of Nucleic Acid Nanostructures. *Nucleic Acids Res.* **2012**, *40*, 2862−2868.
(45) Yoo, J.; Aksimentiev, A. *In Situ* Structure and Dynamics of DNA Origami Determined through Molecular Dynamics Simulations. *Proc. Natl. Acad. Sci. U. S. A.* **2013**, *110*, 20099−20104.
(46) Bai, X.; Martin, T. G.; Scheres, S. H. W.; Dietz, H. Cryo-EM Structure of a 3D DNA-Origami Object. *Proc. Natl. Acad. Sci. U. S. A.* **2012**, *109*, 20012−20017.
(47) Gerling, T.; Wagenbauer, K. F.; Neuner, a. M.; Dietz, H. Dynamic DNA Devices and Assemblies Formed by Shape-Complementary, Non − Base Pairing 3D Components. *Science* **2015**, *347*, 1446−1452.
(48) Fujibayashi, K.; Hariadi, R.; Park, S. H.; Winfree, E.; Murata, S. Toward Reliable Algorithmic Self-Assembly of DNA Tiles: A Fixed-Width Cellular Automaton Pattern. *Nano Lett.* **2008**, *8*, 1791−1797.

DOI: 10.1021/acsnano.5b05309
ACS Nano 2016, 10, 1836−1844